International Journal of Rotating Machinery, 8(1): 13–25, 2002

1023-621X/02 $12.00+.00

Dynamic Behavior of Elastically Tailored Rotating Blades Modeled as Pretwisted Thin-Walled Beams and Incorporating Adaptive Capabilities

OHSEOP SONG[1], SANG-YONG OH[1], and LIVIU LIBRESCU[2,*]
[1]*Chungnam National University, Taejon, South Korea;*
[2]*Virginia Polytechnic Institute and State University, Blacksburg, Virginia 24061, USA*

A number of issues related with the vibrational behavior of rotating blades modeled as pretwisted thin-walled anisotropic beams, incorporating adaptive capabilities are addressed. The adaptive capabilities are provided by a system of piezoactuators bonded or embedded into the structure. Based on the converse piezoelectric effect and on the out-of-phase activation, boundary control moments are piezoelectrically induced at the beam tip. A feedback control law relating the induced bending moments with the kinematical response quantities appropriately selected is used, and its beneficial effects, considered in conjunction with that of the beam anisotropy and structural pretwist upon the closed/open loop eigenvibration characteristics are highlighted.

Keywords: Rotating blades; Thin-walled beams; Adaptive materials; Feedback control; Flapping-lagging motion; Structural tailoring

In the continuous quest for improved efficiency and higher performance of rotorcraft structures and turbomachines operating in severe environmental conditions, there is a stringent need for new paradigms able to enhance the vibrational behavior of these structures.

Enhancement of the dynamic response of these devices would result in higher efficiency and higher thrust-to-weight ratio, lower vibrational levels, lighter rotorcraft structures, with less susceptibility to fatigue failure. Moreover, implementation of the new methods in the turbomachinery for space applications, would result in a considerable increase of their fatigue life.

The design of advanced rotor blades was significantly influenced by the incorporation of composite materials technology. As compared to their metallic counterparts, composite design of rotor blades offers considerable advantages with respect to strength and weight criteria, in addition to providing adequate means of efficiently controlling their static and dynamic response *via* implementation of structural tailoring.

However, in order to enhance their dynamic behavior and avoid vibration-induced fatigue failure, in addition to the tailoring technique which is passive in nature, new technologies have to be implemented. One of the ways to accomplish such goals consists of the incorporation into the host structure of adaptive materials technology. In this case the structures are referred to as *intelligent or smart structures*. In constrast to traditional passive structures, in those featuring adaptive capabilities, the natural frequencies, damping and mode shapes can be tuned to avoid structural reasonance and enhance dynamic response characteristics. In addition, due to the nature of *intelligent structures* which feature a highly distributed network of sensors and actuators, more encompassing feedback control schemes would be feasible to the implemented. For helicopter and tilt rotor aircraft, the incorporation of adaptive materials technology for vibration control could result in significant increases, among others, in comfort, range, fatigue life. In this sense, piezoelectric materials are excellent candidates for the role of sensors and actuators.

Within this study, an investigation of the free vibration of pretwisted rotating blades modeled as thin-walled beams whose material is characterized by anisotropic properties, and incorporating the adaptive capability, referred to as *strain actuation*, will be carried out.

The adaptive capability is achieved through the converse peizoelectric effect consisting of the generation of localized strains in response to an applied voltage. The induced strain field produces, in turn, an adaptive change in the dynamic response characteristics of the structure.

Received 14 December 1999; In final form 7 April 2000.
*Corresponding author. Tel.: 540 231-4574, Fax: 540 231-4574, e-mail: librescu@vt.edu

Implementation of a feedback control law relating the applied electric field to one of the mechanical quantities characterizing the blade response according to a prescribed functional relationship, results in a closed-loop eigenvalue problem. Its solution supplies the closed-loop eigenvalues which are functions of the applied voltage, i.e., of the feedback control gain.

Under consideration is a blade rotating with constant angular velocity and modelled as a pretwisted, single-cell thin/thick walled beam.

Although of an evident practical importance, to the best of the authors' knowledge no studies related to the topic of this investigation can be found in the specialized literature. Even for the *non-adaptive* case, the literature devoted to the free vibration problem of *rotating composite blades modeled as pretwisted thin-walled beams* reveals an extreme paucity of results. The survey-paper, by Rosen (1991), presenting the state of the art in the area of pretwisted rotating blades, and the papers by Sunar and Rao (1999) and Crawley (1994), summarizing the achievements reached in the area of intelligent structures, in general and its prospects of its incorporation in aerospace constructions, respectively, confirm in full this statement. The goal of this paper is to fill the existing gap and supply pertinent information in this area. The results reported herein constitute a generalization and continuation of those previously obtained by Song and Librescu (1993, 1997a, b, c, 1999) and Librescu et al. (1996).

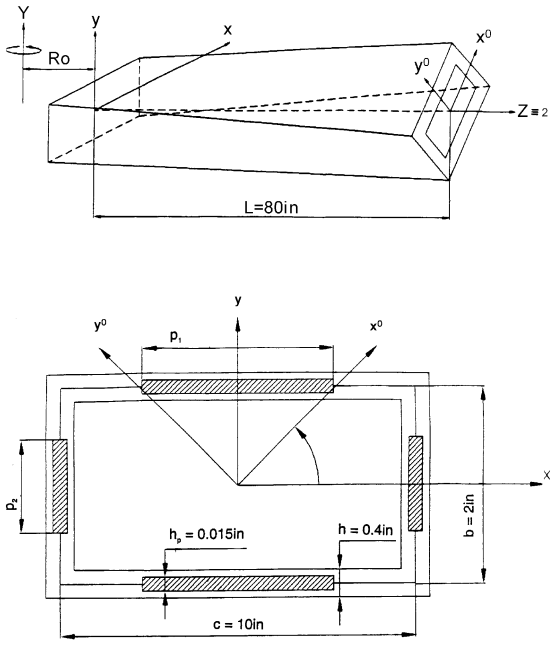

FIGURE 1 Geometry of the pretwisted beam and its cross-section with the embedded piezoactuators.

BASIC ASSUMPTIONS

In the following section, a short account of the basic equations to be used will be presented. Herein, the case of a straight pretwisted flexible beam of length L rotating with the constant angular velocity $\mathbf{\Omega}$ normal to the plane of rotation is considered. The origin of the rotating axis system (x, y, z) is located at the blade root at an offset R_0 from the rotation axis fixed in space. R_0 denotes also the radius of the hub (considered to be rigid), at which the blade is mounted and which rotates about its polar axis through the origin 0 (see Fig. 1).

Besides the coordinates (x, y, z), the local coordinates (x^p, y^p, z^p) are also defined where x^p and y^p are the *principal axes* of an arbitrary beam cross-section Song and Librescu (1997a).

The two coordinate systems are related by the following transformation formulae:

$$\begin{aligned} x(s,z) &= x^p(s)\cos\beta - y^p(s)\sin\beta \\ y(s,z) &= x^p(s)\sin\beta + y^p(s)\cos\beta \qquad [1a-c] \\ z(s) &= z^p \end{aligned}$$

where $\beta(z) = \beta_0 z$, denotes the pretwist of the current section, whereas β_0 denotes the pretwist per unit beam length.

The inertial reference system (X, Y, Z) is attached to the center of the hub O. By (**i**, **j**, **k**) and (**I**, **J**, **K**) we define the unit vectors associated with the frame coordinates (x, y, z) and (X, Y, Z), respectively. In addition, a local (surface) coordinate system (s, z, n) associated with the beam is considered. Its geometric configuration and the typical cross-section along with the associated system of coordinates are presented in Figure 1.

Within the present work, the precone and pre-setting of the blade are assumed to be zero. It is further assumed that the rotation takes place in the plane (X, Z) with the constant angular velocity $\mathbf{\Omega}(\equiv \Omega\mathbf{J} = \Omega\mathbf{j})$, the spin axis being along the Y-axis.

Concerning the beam spanwise z-coordinate axis, it coincides with a straight unspecified reference axis.

Toward its modeling, the following assumptions are adopted: (i) the original cross-section of the beam is preserved, (ii) transverse shear, rotatory inertia and centrifugal accelerations are included, and finally, (iii) a special lay-up inducing flapwise-chordwise bending coupling is implemented.

KINEMATICS

In light of the previously mentioned assumptions, and in order to reduce the 3-D elasticity problem to an equivalent

1-D one, the components of the displacement vector are represented as (see e.g., Librescu et al., 1996, 1997 and Song and Librescu, 1997c).

$$u(x,y,z;t) = u_0(z;t) - y\phi(z;t);$$

$$v(x,y,z;t) = v_0(z;t) + x\phi(z;t),$$

$$w(x,y,z;t) = w_0(z;t) + \theta_x(z;t)\left[y(s) - n\frac{dx}{ds}\right] + \theta_y(z;t)\left[x(s) + n\frac{dy}{ds}\right] - \phi'(z;t)[F_\omega(s) + na(s)]\,. \qquad [2a-c]$$

In these equations $u_0(z;t)$, $v_0(z;t)$, $w_0(z;t)$ denote the rigid body translations along the x, y and z axes while $\phi(z;t)$ and $\theta_x(z;t)$, $\theta_y(z,t)$ denote the elastic twist about the z-axis and the rotations about the x and y-axes, respectively. The expressions of θ_x and θ_y are

$$\theta_x(z;t) = \gamma_{yz}(z;t) - v_0'(z;t); \quad \theta_y(z;t) = \gamma_{xz}(z;t) - u_0'(z;t), \qquad [3a, b]$$

In Eqs. [2], $F_\omega(s)$ and $na(s)$ play the role of primary and secondary warping functions, respectively. For their definition see e.g., Song and Librescu (1993). However, having in view that our analysis will concern the case of rotating thin-walled beams featuring the bending – bending elastic coupling, the quantities associated with the twist ϕ and axial displacement w_0 become immaterial. The terms associated with the twist effect are underscored in Eqs. [2] by an undulated line.

In the absence of transverse shear effects, from Eqs. [3a, b] is readily seen that

$$\theta_x(z;t) = -v_0'(z;t); \quad \theta_y(z;t) = -u_0'(z;t). \qquad [4a, b]$$

In these equations, as well as in the forthcoming ones, the primes denote differentiation with respect to the longitudinal z-coordinate. The position vector of a point $M(x,y,z)$ belonging to the deformed structure is

$$\mathbf{R}(x,y,z;t) = (x+u)\mathbf{i} + (y+v)\mathbf{j} + (z+w)\mathbf{k} + \mathbf{R}_0 \qquad [5]$$

where x, y and z are the Cartesian coordinates of the points of the continuum in its undeformed state, while u, v and w denote displacement components defined through Eqs. [2]. Recalling that the spin rate was assumed to be constant, with the help of equations expressing the time derivatives of unit vectors $(\mathbf{i},\mathbf{j},\mathbf{k})$, one obtain the velocity and acceleration vectors of an arbitrary point M of the beams under the form

$$\dot{\mathbf{R}} = V_x\mathbf{i} + V_y\mathbf{j} + V_z\mathbf{k} \qquad [6a]$$

and

$$\ddot{\mathbf{R}} = a_x\mathbf{i} + a_y\mathbf{j} + a_z\mathbf{k} \qquad [6b]$$

respectively, where their components are as follows:

$$V_x = \dot{u} + (R_0 + z + w)\Omega; \quad V_y = \dot{v}, \quad V_z = \dot{w} - (x+u)\Omega \qquad [7a-c]$$

and

$$a_x = \ddot{u} + 2\dot{w}\Omega - \underline{\underline{(x+u)\Omega^2}}; \quad a_y = \ddot{v}, \quad a_z = \ddot{w} - 2\dot{u}\Omega - \underline{\underline{(R_0 + z + w)\Omega^2}} \qquad [8a-c]$$

In these equations and the following ones, the superposed dots denote time derivatives, whereas the terms underscored by one or two superposed solid lines are associated with Coriolis and centrifugal inertia terms, respectively.

EQUATIONS OF MOTION AND BOUNDARY CONDITIONS

The equations of motion of rotating pretwisted beams and the associated boundary conditions, can be obtained via the application of Hamilton's variational principle.

In various contexts related with the dynamic modeling of thin-walled beam, this principle was thoroughly used (see e.g., Song and Librescu, 1993, 1997a, b, c, 1999 and Librescu et al., 1996, 1997) and for this reason, herein, only the basic steps enabling one to get the final governing equations will be outlined.

The governing system of elastic rotating blades will be expressed, as is customary, in terms of displacement quantitites. This can be accomplished by replacing in the equations of motion and static boundary conditions the 1-D stress-resultants and stress-couples represented in terms of displacement quantities. All these steps are not carried out here.

For the general case of anisotropy of constituent materials and ply-stacking sequence, the obtained governing system and the associated boundary conditions would exhibit a complete coupling between the various modes, i.e., warping (primary and secondary), bending (flapping and lagging), twist, extension and transverse shearing. The assessment of the influence of these couplings and their proper exploitation (see e.g., Librescu et al., 1996, 1997 and Song and Librescu, 1997c) should constitute an important task towards a rational design of blade structures of

helicopter and tilt rotor aircraft and of the proper use of the exotic material characteristics (i.e., anisotropy and ply-stacking sequence) generating these couplings.

Moreover, due to inclusion of the pretwist, additional couplings are induced, which in such a general context, would add additional complexities to the problem (see e.g., Kosmatka, 1992). For these reasons, in the present analysis a special ply-angle distribution inducing the elastic coupling between flapwise bending and chordwise bending, (referred also to as flap-lag or bending–bending cross coupling), will be considered. On the other hand, having in view that Coriolis effect induces a coupling with the extensional motion and since its contribution is considered to be negligeable, (see e.g., Ewins and Henry, 1992), this effect will be discarded. This ply-angle distribution referred to as *circumferentially uniform stiffness* (CUS) configuration is achieved by skewing angle plies with respect to the beam axis according to the law $\theta(y)=\theta(-y)$ in the top and bottom flanges, and to the law $\theta(x)=\theta(-x)$ in the lateral webs. Angle θ denotes the dominant ply orientation measured from the positive s-axis towards the positive z-axis. Consistent with this ply-angle configuration, the following *governing equations* incorporating transverse shear effects and coupling the flapwise and chordwise bendings are obtained:

$$
\begin{aligned}
\delta u_0 &: [a_{43}(z)\theta_x' + a_{44}(z)(u_0' + \theta_y) \\
&\quad + a_{45}(z)(v_0' + \theta_x)]' \\
&\quad - b_1\ddot{u}_0 + \underline{b_1 u_0\Omega^2} + \underline{\underline{b_1\Omega^2[R(z)u_0']'}} = 0, \\
\delta v_0 &: [a_{52}(z)\theta_y' + a_{55}(z)(v_0' + \theta_x) \\
&\quad + a_{45}(z)(u_0' + \theta_y)]' \\
&\quad - b_1\ddot{v}_0 + \underline{\underline{b_1\Omega^2[R(z)v_0']'}} = 0, \\
\delta\theta_y &: [a_{22}(z)\theta_y' + a_{25}(z)(v_0' + \theta_x) + a_{23}(z)\theta_x']' \\
&\quad - a_{44}(z)(u_0' + \theta_y) - a_{43}(z)\theta_x' \\
&\quad - a_{45}(z)(v_0' + \theta_x) \\
&\quad - (b_5(z) + b_{15}(z))(\ddot{\theta}_y - \underline{\underline{\Omega^2\theta_y}}) \\
&\quad - (b_6(z) - b_{13}(z))\ddot{\theta}_x = 0, \\
\delta\theta_x &: [a_{33}(z)\theta_x' + a_{23}(z)\theta_y' + a_{34}(z)(u_0' + \theta_y)]' \\
&\quad - a_{55}(z)(v_0' + \theta_x) - a_{52}(z)\theta_y' \\
&\quad - a_{54}(z)(u_0' + \theta_y) \\
&\quad - (b_4(z) + b_{14}(z))(\ddot{\theta}_x - \underline{\underline{\Omega^2\theta_x}}) \\
&\quad - (b_6(z) - b_{13}(z))(\ddot{\theta}_y - \underline{\underline{\Omega^2\theta_y}}) = 0.
\end{aligned}
\qquad [9a-d]
$$

In addition, assuming the blade to be clamped at $z=0$ and free at $z=L$, the boundary conditions result as:
At $z=0$

$$
u_0 = 0, \quad v_0 = 0, \ \theta_x = 0, \ \theta_y = 0 \qquad [10a-d]
$$

and at $z=L$:

$$
\begin{aligned}
\delta u_0 &: a_{43}(z)\theta_x' + a_{44}(z)(u_0' + \theta_y) \\
&\quad + a_{45}(z)(v_0' + \theta_x) = 0, \\
\delta v_0 &: a_{52}(z)\theta_y' + a_{55}(z)(v_0' + \theta_x) \\
&\quad + a_{45}(z)(u_0' + \theta_y) = 0, \\
\delta\theta_y &: a_{22}(z)\theta_y' + a_{25}(z)(v_0' + \theta_x) \\
&\quad + a_{23}(z)\theta_x' = \hat{M}_y, \\
\delta\theta_x &: a_{33}(z)\theta_x' + a_{34}(z)(u_0' + \theta_y) \\
&\quad + a_{23}(z)\theta_y' = \hat{M}_x.
\end{aligned}
\qquad [11a-d]
$$

In these equations (see Song and Librescu, 1997a)

$$
R(z) \equiv \left[R_0(L-z) + \frac{1}{2}(L^2 - z^2)\right], \qquad [12]
$$

whereas the coefficients $a_{ij}(z)=a_{ji}(z)$ and $b_i(z)$ denote stiffness and reduced mass terms, respectively.

The expressions of stiffness quantities in terms of their cross-section principal axes (x^p, y^p) counterparts are recorded in the Appendix, together with those of the mass terms. Equations [9] and [11] reveal that in the context of above considered ply-angle configuration, the flapwise and chordwise bending are coupled with transverse shear. For this case, the coupling stiffnesses a_{34} and a_{25} are a reflect of this ply angle configuration. In addition, the stiffness quantities a_{45} and a_{23} and the mass terms b_6 and b_{13} which are different from zero only in the case of a pretwisted beam, induce a supplementary coupling between the flapwise and chordwise motions. However, from the expressions of a_{45}, a_{23}, b_6 and b_{13} (see the Appendix), it can readily be seen that for an axisymmetric box-beam of a *square cross-section*, these quantities vanish for any value of β. As a result, in such a case, the flapwise-chordwise coupling arises independently from the pretwist effect. It should also be remarked that in addition to the above mentioned coupling terms generated by pretwist, the remaining ones involve, as a result of it, a more complex feature. Their expressions displayed in Appendix substantiates in full this statement.

Notice that in addition to the above mentioned elastic couplings induced by the above ply-angle distribution and the pretwist, Eqs. [9] through [11] feature also the coupling between the flapwise shear and chordwise bending and between chordwise shear and flapwise bending. Moreover, the above governing equation system includes also the centrifugal and rotatory inertia effects.

The system of Eqs. [9] through [11] corresponds to the *shearable beam model*, whereas its classical counterpart obtained when transverse shear effects are discarded, is referred to as the *nonshearable model*. Within the theory of

solid beams, this model is referred to as Bernoulli–Euler–Rayleigh model. It should be mentioned that in the expressions of transverse shear stress resultants intervening in the equations of motion, a transverse shear correction factor $k^2 = 5/6$ was used.

NONSHEARABLE BEAM MODEL COUNTERPART

Elimination of $a_{44}(u_0' + \theta_y) + a_{45}(u_0{}' + \theta_x)$ and of $a_{55}(v_0' + \theta_x) + a_{54}(u_0' + \theta_y)$ in the groups of Eqs. [9a, c] and [9b, d], respectively, followed by consideration of $\theta_x \to -v_0'$ and $\theta_y = -u_0'$, yields the Bernoulli–Euler–Rayleigh counterpart of Eqs. [9] through [11]. As a result, the governing equations result as:

$$\begin{aligned}
\delta u_0 : {} & [a_{22}(z)u_0'' + a_{23}(z)v_0'']'' \\
& - [(b_5(z) + b_{15}(z))(\ddot{u}_0' \underline{\underline{-\Omega^2 u_0'}}) \\
& \quad - (b_6(z) - b_{13}(z))\ddot{v}_0']' \\
& + b_1\ddot{u}_0 \underline{\underline{-b_1\Omega^2 u_0}} - \underline{\underline{b_1\Omega^2[R(z)u_0']'}} = 0, \\
\delta v_0 : {} & [a_{33}(z)v_0'' + a_{23}(z)u_0'']'' \\
& - [(b_4(z) + b_{14}(z))(\ddot{v}_0' \underline{\underline{-\Omega^2 v_0'}}) \\
& \quad + (b_6(z) - b_{13}(z))(\ddot{u}_0' - \underline{\underline{\Omega^2 u_0'}})]' \\
& - b_1\ddot{v}_0 - \underline{\underline{b_1\Omega^2[R(z)v_0']'}} = 0.
\end{aligned} \qquad [13a, b]$$

The associated boundary conditions are:

At $z = 0$

$$u_0 = v_0 = u_0' = v_0' = 0 \qquad [14a - d]$$

and at $z = L$:

$$\begin{aligned}
\delta u_0 : {} & [a_{22}(z)u_0'' + a_{23}(z)v_0'']' \\
& - [(b_5(z) + b_{15}(z))(\ddot{u}_0' \underline{\underline{-\Omega^2 u_0'}}) \\
& \quad - (b_6(z) - b_{13}(z))\ddot{v}_0'] = 0, \\
\delta v_0 : {} & [a_{33}(z)v_0'' + a_{23}(z)u_0'']' \\
& - [(b_4(z) + b_{14}(z))(\ddot{v}_0' \underline{\underline{-\Omega^2 v_0'}}) \\
& \quad + (b_6(z) - b_{13}(z))(\ddot{u}_0' \underline{\underline{-\Omega^2 u_0'}})] = 0, \\
\delta u_0' : {} & a_{22}(z)u_0'' + a_{23}(z)v_0'' = \hat{M}_y, \\
\delta v_0' : {} & a_{33}(z)v_0'' + a_{32}(z)u_0'' = \hat{M}_x.
\end{aligned} \qquad [15a - d]$$

In this case, the only flapping–lagging coupling stiffness induced by the pretwist effect is $a_{23}(z)$, whereas, $(b_6(z) - b_{13}(z))$ represents the dynamic flapping–lagging coupling term induced by pretwist.

Consistent with the number of four boundary conditions at each edge, the governing equations for both shearable and unshearable pretwisted rotating beams are of the eight order. A noticeable difference between the shearable and unshearable beam models consists of the fact that in the former instance, in the boundary conditions at the tip the eigenfrequencies do not intervene, whereas in the latter one, these occur.

In Eqs. [11c, d] and their non-shearable counterparts, Eqs. [15b, d], $\hat{M}_y$ and $\hat{M}_x$ stand for the piezoelectrically induced bending moments about the axes y and x, respectively, that appear as non-homogeneous terms in the boundary conditions at $z = L$. It should be noticed that $\hat{M}_x$ and $\hat{M}_y$ are different from zero, only if external voltages of opposite signs are applied on the top and bottom, and in the lateral piezoactuator layers, respectively (out-of-phase activation).

It should be remarked that in the light of the actuator configuration, the piezoelectrically induced stress-resultant and stress-couples are independent upon the z-coordinate. As a result, in the governing equations their contribution is immaterial while in the boundary conditions they intervene as non-homogeneous terms, only. This feature renders the control to be accomplished *via* the piezoelectrically induced *boundary bending moments*. At this point it should be noticed that the feedback boundary control constitutes a powerful way to control the static and dynamic response of structures (see Librescu et al., 1996, 1997, 1999 and Librescu and Na, 1998).

PIEZOACTUATORS AND CONTROL LAW

It is assumed that the master structure is composed of r layers while the actuator is composed of p piezoelectric layers. We stipulate that the actuators are distributed over the entire span of the blade, whereas along the circumferential and transverse directions, i.e., along the s- and n-directions are distributed according to the law

$$\begin{aligned}
P_{(k)}(n) &= H(n - n_{(k^-)}) - H(n - n_{(k^+)}), \\
P_{(k)}(s) &= H(s - s_{(k^-)}) - H(s - s_{(k^+)}).
\end{aligned} \qquad [16]$$

Herein H denotes Heaviside's distribution, P is a spatial function which defines the distribution of actuators in the n and the s directions, and the subscript k identifies the affiliation of the respective quantity to the kth layer.

Assuming that the electric field vector $\mathcal{E}_i$ is represented by its component $\mathcal{E}_3$ in the n-direction, coinciding with the direction of polarization (referred to as thickness

polarization), the boundary moment controls are expressed as

$$\hat{M}_x = \oint \sum_{k=1}^{p} \mathcal{E}_3^{(k)} \left(n_{(k^+)} - n_{(k^-)}\right) e_{31}^{(k)} P_{(k)}(s) \left[y\left(1 - \frac{\hat{A}_{12}}{\hat{A}_{11}}\right) + \frac{dx}{ds}\frac{\hat{B}_{12}}{\hat{A}_{11}} \right] ds - \frac{1}{2}\oint \left[\frac{dx}{ds} \sum_{k=1}^{p} \mathcal{E}_3^{(k)} \left(n_{(k^+)}^2 - n_{(k^-)}^2\right) e_{31}^{(k)} P_{(k)}(s) \right] ds,$$

$$\hat{M}_y = \oint \sum_{k=1}^{p} \mathcal{E}_3^{(k)} \left(n_{(k^+)} - n_{(k^-)}\right) e_{31}^{(k)} P_{(k)}(s) \left[x\left(1 - \frac{\hat{A}_{12}}{\hat{A}_{11}}\right) + \frac{dy}{ds}\frac{\hat{B}_{12}}{\hat{A}_{11}} \right] ds + \frac{1}{2}\oint \left[\frac{dy}{ds} \sum_{k=1}^{p} \mathcal{E}_3^{(k)} \left(n_{(k^+)}^2 - n_{(k^-)}^2\right) e_{31}^{(k)} P_{(k)}(s) \right] ds. \quad [17a, b]$$

Herein e_{31} is the piezoelectric constant; $\hat{A}_{ij}$ and $\hat{B}_{ij}$ are the standard local-stiffness quantities associated with the piezoactuators, while $\oint(\cdot)ds$ denotes the integral around the circumference of the mid-line cross-section of the beam.

For $\mathcal{E}_3$ constant throughout the piezoactuator thickness, this implying $\mathcal{E}_3^{(k)} \equiv \mathcal{E}_3$, Eqs. [17] can be expressed in condensed form as:

$$\hat{M}_x = \mathcal{E}_3 \mathcal{M}_x, \quad \hat{M}_y = \mathcal{E}_3 \mathcal{M}_y \quad [18a, b]$$

where the meaning of $\mathcal{M}_x$ and $\mathcal{M}_y$ becomes evident by comparing Eqs. [18] with [17].

Equations [17] reveal that the piezoelectrically induced bending moments are proportional to the applied electric field $\mathcal{E}_3$. Now, assuming that the piezoelectric elements can be employed concurrently for sensing and actuation, for sensing operation the electric displacement results as

$$D_3 = e_{31} S_{zz}, \quad [19]$$

and the sensor output voltage is expressed in the form (see Dosch et al., 1992)

$$V_s(t) = \frac{q_s(t)}{C_p}, \quad [20]$$

where the electric charge $q_s(t)$ is

$$q_s(t) = \int_{A_s} D_3 dA_s = \int_{A_s} e_{31} S_{zz} dA_s, \quad [21]$$

C_p and A_s denoting the sensor's capacitance and piezoelectric patch area, respectively, while S_{zz} denotes the axial strain component (see Song and Librescu, 1993 and Librescu et al., 1997). Assuming the sensor patches being located symmetrically on the opposite walls, i.e., on $y = \pm b/2$ and $x = \pm c/2$, having in view the expression of S_{zz} and Eqs. [19] through [21], $V_s^x(t)$ and $V_s^y(t)$ are expressible as:

$$V_s^x(t) = C_x^s \theta_x(L,t), \quad V_s^y(t) = C_y^s \theta_y(L,t) \quad [22a, b]$$

where the expressions of C_y^s and C_x^s are not displayed here.

The feedback control law to be used here is referred to as *the proportional feedback control law*.

Within this control law, one postulates that the actuating electric field is proportional to the sensor output voltage, which implies

$$\mathcal{E}_3^x(t) = K_p V_s^x(t)/h_a, \quad \mathcal{E}_3^y(t) = K_p V_s^y(t)/h_a \quad [23a, b]$$

where h_a is the thickness of the piezopatch.

Consequently, replacement of Eqs. [23] considered in conjunction with Eqs. [22] into Eqs. [18] results in the piezoelectrically induced bending moments expressed as:

$$\hat{M}_y(L,t) = \frac{K_p C_{M_y^a}}{h_a} [C_y^s \theta_y(L,t)] = K_p C_{11} \theta_y(L,t), \quad [24a]$$

$$\hat{M}_x(L,t) = \frac{K_p C_{M_x^a}}{h_a} [C_x^s \theta_x(L,t)] = K_p C_{22} \theta_x(L,t). \quad [24b]$$

The results yielding the piezoelectrically induced bending moments, Eqs. [24], reveal that these are obtained through the combination of both sensing and actuation functions.

Herein

$$C_{M_y^a} = \sum_{k=1}^{r} e_{31}^{(k)} \left[\left(1 - \frac{\hat{A}_{11}}{\hat{A}_{11}}\right) \left(n_{(k^+)} - n_{(k^-)}\right) c + \left(n_{(k^+)}^2 - n_{(k^-)}^2\right) - 2\frac{\hat{B}_{12}}{\hat{A}_{11}} \left(n_{(k^+)} - n_{(k^-)}\right) \right] p_2, \quad [25a]$$

$$C_{M_x^a} = \sum_{k=1}^{r} e_{31}^{(k)} \left[\left(1 - \frac{\hat{A}_{11}}{\hat{A}_{12}}\right) \left(n_{(k^+)} - n_{(k^-)}\right) b + \left(n_{(k^+)}^2 - n_{(k^-)}^2\right) - 2\frac{\hat{B}_{12}}{\hat{A}_{11}} \left(n_{(k^+)} - n_{(k^-)}\right) \right] p_1 \quad [25b]$$

where p_1 and p_2 denote the lengths of the piezoactuators along the x- and y-directions (see Figure 1b), while r stands for the number of piezoactuator layers.

As concerns the proportional feedback gain K_p, this will be used in dimensionless form as:

$$\overline{K}_p = \frac{K_p L}{\hat{a}_{33} h_p} \tag{26}$$

where $\hat{a}_{33}$ is the transverse bending stiffness corresponding to the ply-angle $\theta = 0$.

The eigenvalue problem involving the coupled governing Eq. [9] considered in conjunction with the boundary conditions Eqs. [10] and [11], and the control law, Eqs. [24], yields the closed-loop eigenvalue problem related to the problem of rotating thin-walled beams.

THE DISCRETIZED GOVERNING EQUATIONS OF THE ADAPTIVE ROTATING BEAM

For practical purposes, it is necessary to discretize the eigenvalue-value problem. This amounts to representing u_0, v_0, θ_x and θ_y by means of series of space-dependent trial functions multiplied by time-dependent generalized coordinates. The discretization can be conveniently performed via the Extended Galerkin's Method (see e.g., Librescu et al., 1996, 1997 and Song and Librescu, 1997c). To this end, we express the displacements as:

$$\begin{aligned} u_0(z,t) &= \mathbf{U}_0^T(z)\mathbf{q}_u(t), \quad v_0(z,t) = \mathbf{V}_0^T(z)\mathbf{q}_v(t) \\ \theta_x(z,t) &= \mathbf{X}_0^T(z)\mathbf{q}_x(t), \quad \theta_y(z,t) = \mathbf{Y}_0^T(z)\mathbf{q}_y(t). \end{aligned} \tag{27a - d}$$

where

$$\begin{aligned} \mathbf{U}_0(z) &= [u_1 u_2 \dots u_N]^T, \quad \mathbf{V}_0(z) = [v_1 v_2 \dots v_N]^T \\ \mathbf{X}_0(z) &= [x_1 x_2 \dots x_N]^T, \quad \mathbf{Y}_0(z) = [y_1 y_2 \dots y_N]^T \end{aligned} \tag{28a - d}$$

are the vectors of the space-dependent trial functions, selected as to fulfil at least the geometric boundary conditions, whereas for free-vibration problem $\mathbf{q}_u(t)$, $\mathbf{q}_v(t)$, $\mathbf{q}_x(t)$ and $\mathbf{q}_y(t)$ are represented generically as

$$\mathbf{F}(t) = \overline{\mathbf{F}} e^{\lambda t} \tag{29}$$

where $\overline{\mathbf{F}}$ and λ are constants, both generally complex.

In the activated case

$$(\lambda_r, \overline{\lambda}_r) = \pm i\omega_r \tag{30}$$

where ω_r is the rth frequency of oscillations.

For the problem at hand the trail functions have been selected as polynomials in the z-coordinate that identically fulfil at least boundary conditions [10a–d] or [14a–d], depending on whether the shearable or unshearable beam models are considered, respectively.

NUMERICAL SIMULATIONS AND DISCUSSION

Although the obtained equations are valid for a beam of arbitrary closed-cross section, for the sake of illustration the case of a rotating beam modelled as a composite box-beam (see Figure 1) characterized by a cross-section ratio $\mathcal{R}(\equiv c/b) = 5$ was considered. Depending on whether the flapping, lagging or flapping–lagging coupled motions are intended to be controlled, the piezoactuator layers (selected to be of PZT-4) should be located on the top and bottom flanges, on the opposite lateral webs of the master structure, or on both the flanges and webs, respectively.

While the geometric characteristics of the structure are displayed in Figure 1, the properties of the PZT-4 piezoceramic can be found in Berlincourt et al. (1964) (pp. 202–204), whereas those of the host structure correspond to a graphite/epoxy material, whose mechanical characteristics in the on-axis configuration can be found in the papers by Song and Librescu (1993, 1997).

At this point it should be mentioned that in spite of the extensive work and results devoted to eigenvibration response of pretwisted rotating and non-rotating blades modeled as solid isotropic beams and incorporating bending–bending cross-coupling, to the best of the author's knowledge there are no available results associated with both *adaptive and non-adaptive anisotropic pretwisted rotating thin-walled beams*.

For this reason, before presenting results revealing the effects of anisotropy coupled with that of the pretwist and of induced strain actuation on dynamics of thin-walled rotating blades, a number of results related to the behavior of unactivated rotating/nonrotating blades will be supplied.

In Figures 2a through 2c, there are displayed in succession the variations of the first three eigenfrequencies as a function of the pretwist angle, for selected values of the blade rotational speed.

Having in view that in these cases the ply-angle $\theta = 45°$, it results that the frequencies correspond to the flap–lag coupled motion. Moreover, as it was shown previously, this coupling occurs also in the case of the pretwisted beams.

The trend as emerging from these plots coincides with that reported in the paper by Subrahmanyam and Kaza (1986) and Subrahmanyam et al. (1981) in the case of the blade modeled as a solid isotropic beam.

Figures 3 and 4 highlight the effects of rotational velocity Ω considered in conjunction with that of the proportional feedback control on the first two decoupled natural frequencies in flapping and lagging occuring at the ply-angle $\theta = 0°$. The results reveal that at moderate rotational speeds, the first flapwise mode exhibits the lowest frequency. However, due to the centrifugal stiffening effect

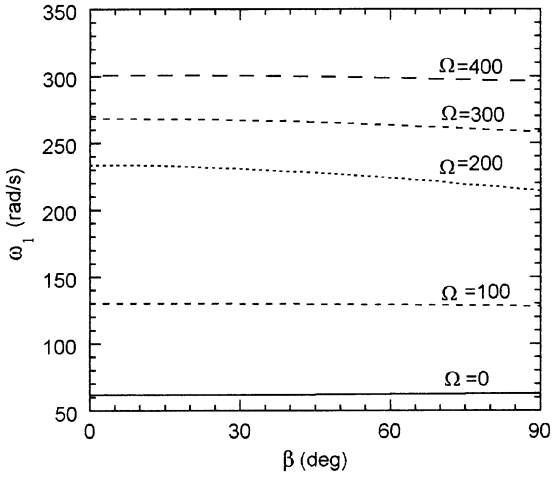

FIGURE 2a Variation of first coupled flapping–lagging natural frequency *vs.* pretwist angle for selected rotational speeds ($\theta = 45°$).

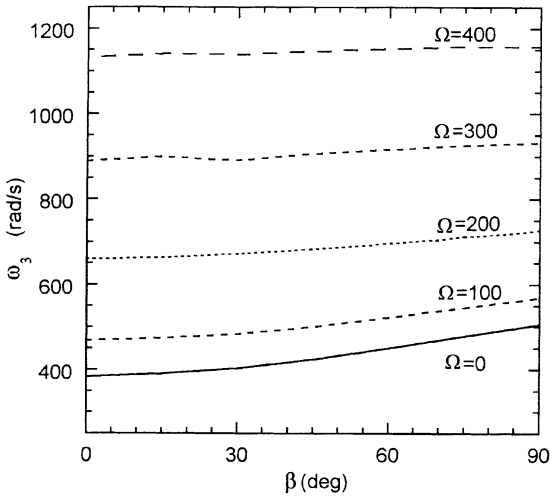

FIGURE 2c Counterpart of Figure 2a for the third coupled mode frequency.

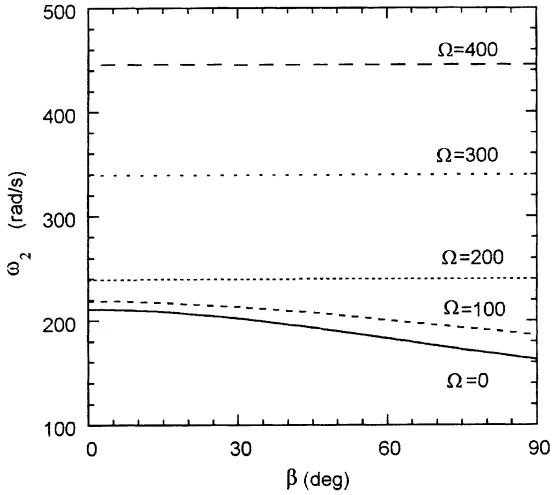

FIGURE 2b Counterpart of Figure 2a for the second coupled mode frequency.

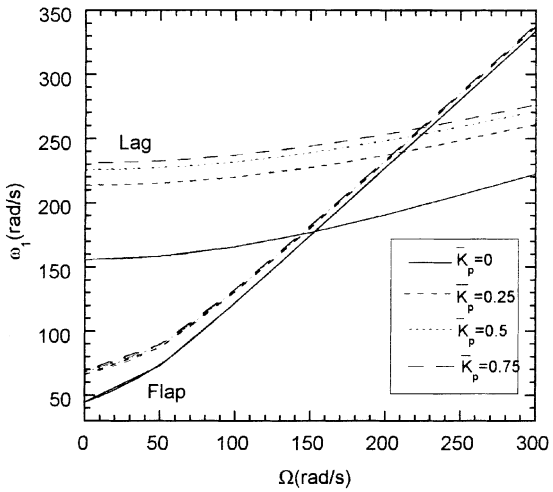

FIGURE 3 Variation of first decoupled flapping and lagging natural frequencies *vs.* rotational speed for selected $\bar{K}_p(\theta = 0°, \beta = 0°)$.

(which is much more significant in the flapping modes), beyond a certain angular speed the lagging frequency becomes the lower of the two. Figure 3 reveals that for the unactivated beam (case corresponding to $\bar{K}_p = 0$), in the vicinity of $\Omega \doteq 150$ rad/sec, a frequency crossing of lagging and flapping modes occurs.

The results also reveal that for the *activated beams* (i.e., for $\bar{K}_p \neq 0$), the frequency crossing is shifted towards larger rotational velocities. At the same time, the supplied results show that the piezoelectric actuation has a more powerful effect on the lagging eigenfrequencies than on the flapping ones. This trend remains still valid for higher mode frequencies.

Moreover, as Figure 4 reveals, for the second mode frequency, the flapping–lagging frequency crossing occurs at much larger values of Ω as compared to that occuring for the fundamental frequencies. It should also be observed that for second mode frequency, the piezoelectric actuation becomes efficient for the flapping frequencies as well. Associated with the ply-angle $\theta = 90°$ the variation of the first mode frequency with Ω as displayed in Figure 5, reveals a similar trend to that supplied in Figure 3 for $\theta = 0°$. In this case, however, due to the larger bending stiffnesses a_{33} and a_{22} in flapping and lagging as induced by this ply-angle, (see Librescu et al., 1996), the frequencies are much higher within the entire range of rotational speeds than their counterparts corresponding to $\theta = 0°$. In addition, the frequency crossings for both the unactivated and the activated rotor blade take place at much larger rotational speeds. In the case of higher mode numbers,

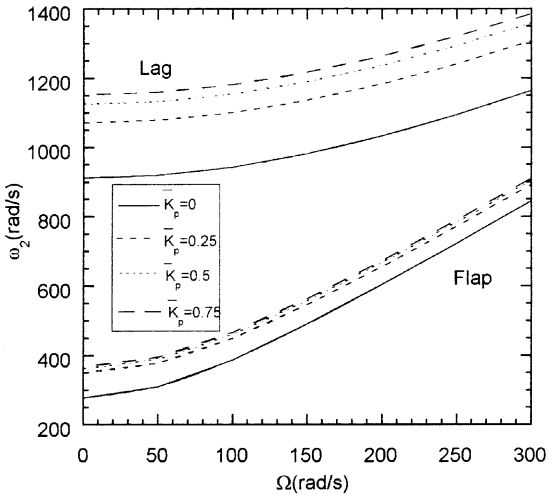

FIGURE 4 Variation of second decoupled flapping and lagging natural frequencies *vs.* rotational speed for selected $\overline{K}_p(\theta = 90°, \beta = 0°)$.

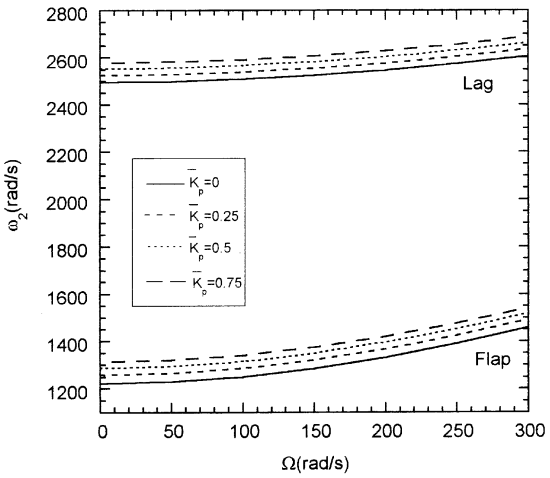

FIGURE 6 Variation of second decoupled flapping and lagging natural frequencies *vs.* rotational speed for selected $\overline{K}_p(\theta = 90°, \beta = 0°)$.

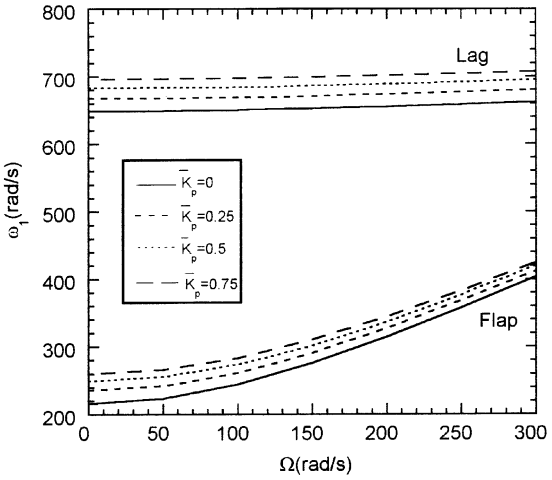

FIGURE 5 Variation of first decoupled flapping and lagging natural frequencies *vs.* rotational speed for selected $\overline{K}_p(\theta = 90°, \beta = 0°)$.

(see Figure 6), the frequencies remain separated in the usual range of rotational speeds, in the sense that no frequency crossings occur in that range.

The comparison of the results obtained for the ply-angle $\theta = 90°$, (Figures 5 and 6), with their counterparts obtained for $\theta = 0°$, Figures 3 and 4, reveals that in the former case the increase of the rotational speed plays a more modest role in increasing the frequencies in flapping and lagging, as compared to the latter case. The trend is due to the increased bending structural stiffness in both flapping and lagging induced by the increase of the ply-angle θ, increase that renders the centrifugal stiffening weaker than in the case of lower bending structural stiffnesses.

In addition, due to the previously emphasized reasons, the same plots reveal that at $\theta = 90°$ the piezoelectric actuation efficiency is lower (in percentage of increase of eigenfrequencies) than that manifested at $\theta = 0°$.

Variation with Ω of the first two coupled eigenfrequencies in flapping-lagging in the case of the implementation of the proportional feedback control is depicted in Figures 7 and 8. The results displayed in these figures have been generated for a ply-angle $\theta = 45°$, and zero-pretwist. The discontinuities in slope in these figures are attributable to the fact that in Figure 7, for this mode, an abrupt change from the flapping dominated motion to the lagging one, whereas in Figure 8 from the lagging dominated one to the flapping motion are occuring. For the unactivated case, the trend of variation of frequencies with the rotational speed, for the indicated ply-angle is in perfect agreement with that

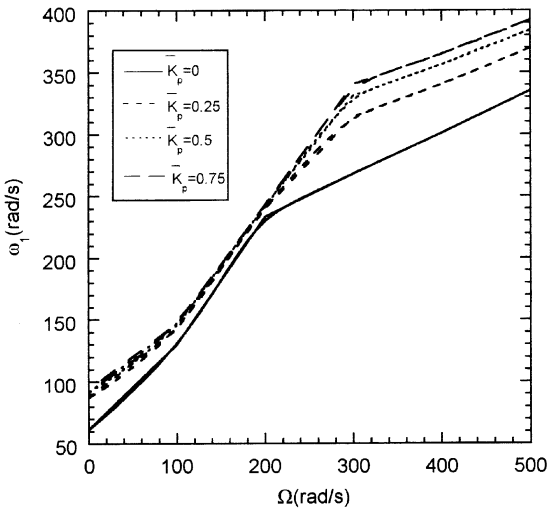

FIGURE 7 Variation of the first coupled flapping–lagging natural frequency *vs.* Ω for selected values of $\overline{K}_p(\beta = 0°, \theta = 45°)$.

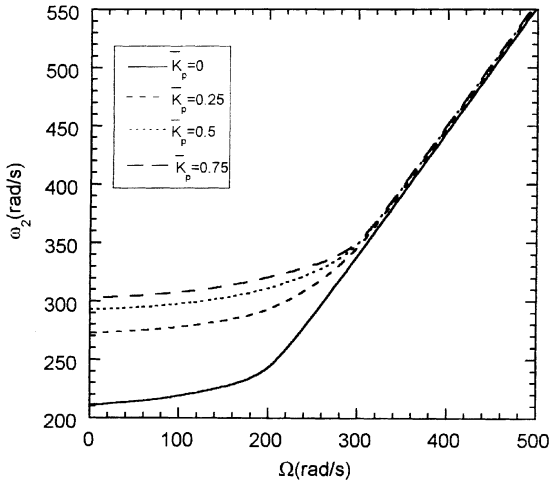

FIGURE 8 Variation of the second coupled flapping–lagging natural frequency *vs.* Ω for selected values of $\overline{K}_p(\beta = 0°, \theta = 45°)$.

reported in Song and Librescu (1997b). In addition, the results of these plots reveal that for the first natural frequency the efficiency of activation is more powerful at larger rotational speeds, whereas for the second eigenfrequency the opposite trend appears to be valid.

Although coupled, the trend of variation of frequencies as emerging from Figures 7 and 8 is consistent with that in Figures 3 and 4 (where the eigenfrequencies are decoupled), in the sense that in Figure 7 beyond $\Omega \doteq 200$ rad/s the lagging motion is the dominant one, whereas in Figure 8, beyond $\Omega \doteq 250$ rad/s the flapping motion is the dominant one.

The effect of the pretwist coupled with that of the beam orthotropy and activation on the variation of the first two coupled eigenfrequencies of a rotating blade is displayed in Figures 9 and 10.

For the unactivated beam, the trend of variation of eigenfrequencies as a function of the pretwist angle is consistent with that reported in the literature in the case of an isotropic solid beam (see Subrahmanyam and Kaza, 1986; Subrahmanyam et al., 1981; Slyper, 1962; Dokumiaci et al., 1967), and also with that emerging from Figures 2a and 2b, displayed in this paper. On the other hand, while the first eigenfrequency is less sensitive mainly to the variation of the feedback gain and less to the pretwist, the second coupled eigenfrequency appears to be sensitive to both effects, i.e., pretwist and piezoelectric actuation. The synergistic implications of implementation of both the tailoring and piezoelectric activation on the first two coupled eigenfrequencies of an untwisted rotating blade ($\Omega = 100$ rad/s, $\beta = 0$), are displayed in Figures 11 and 12. The results displayed reveal that, the tailoring technique coupled with that of the piezoelectric actuation can play a major role toward enhancing the dynamic response of rotating blades.

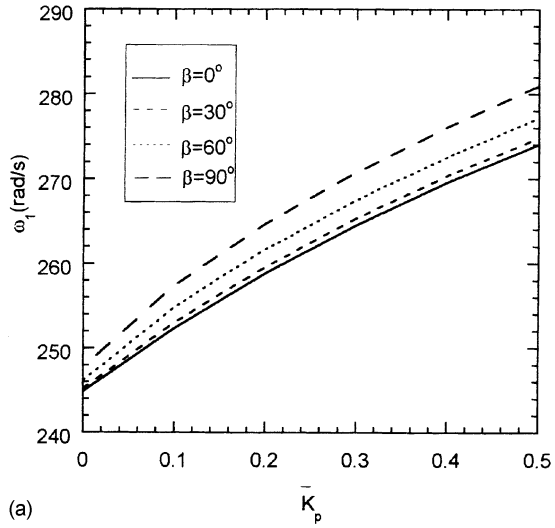

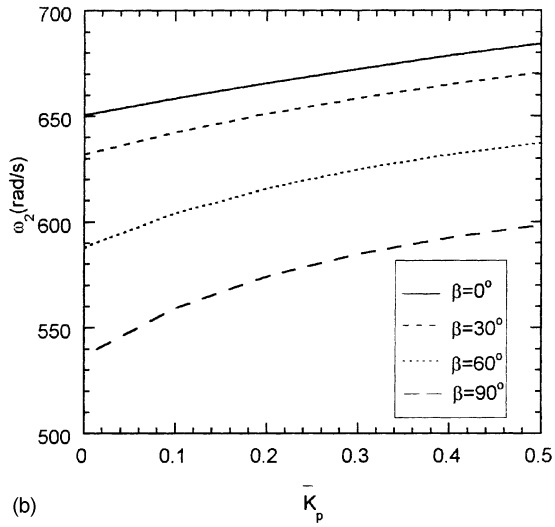

FIGURE 9 Variation of the first two coupled flapping–lagging natural frequencies *vs.* $\overline{K}_p$ for selected values of the total pretwist angle. ($\theta = 90°$, $\Omega = 100$ rad/s). (a) Variation of ω_1, (b) Variation of ω_2.

In order to assess the implications of transverse shear effects, in Figure 13 a comparisons of the variation of the first and second open/closed loop eigenfrequencies of the untwisted rotating blade for the shearable and unshearable blade models as a function of the proportional feedback gain $\overline{K}_p$ is displayed. The results reveal that the unshearable (classical) model overestimates the natural frequencies for both the unactivated ($\overline{K}_p = 0$) and activated ($\overline{K}_p \neq 0$) systems. Moreover, as it appears, the higher mode eigenfrequencies are stronger affected by the transverse shear effect than the lower ones, a trend that is exacerbated with the increase of the feedback gain $\overline{K}_p$.

Finally, in Figure 14 the convergence of the solution carried out via the Extended Galerkin Method, as a

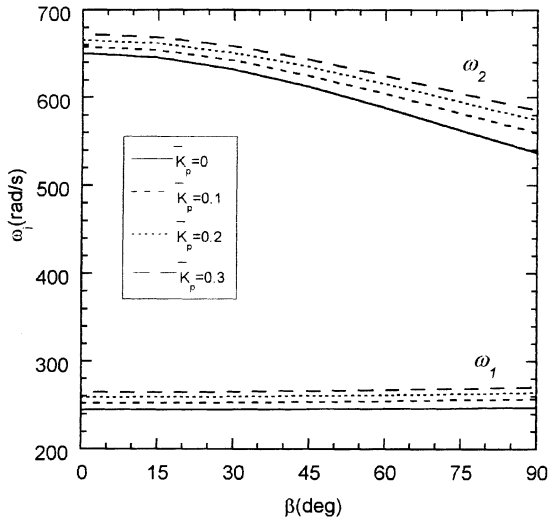

FIGURE 10 Variation of the first two coupled flapping–lagging eigenfrequencies *versus* the total pretwist angle for selected values of the feedback gain $\overline{K}_p(\theta = 90°, \Omega = 100\,\text{rad/s})$.

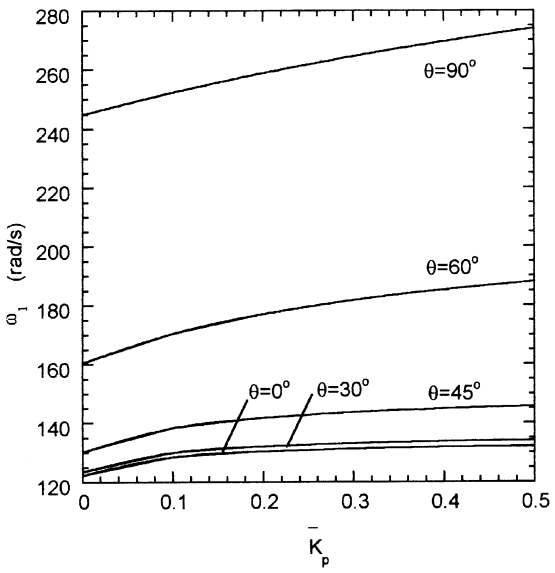

FIGURE 11 Variation of the first coupled flap–lag eigenfrequency *versus* $\overline{K}_p$ for selected values of the ply-angle, ($\beta = 0°$, $\Omega = 100\,\text{rad/s}$).

function of the considered number of terms is displayed. Herein, the variation of the coupled fundamental eigenfrequency *vs.* the rotational speed for the unactivated ($\overline{K}_p = 0$) blade was considered.

The results of this graph reveal, on one hand, the extremely fast convergence of the numerical methodology and, on the other hand, the fact that with only five terms, results in excellent agreement with those obtained by considering more terms can be reached.

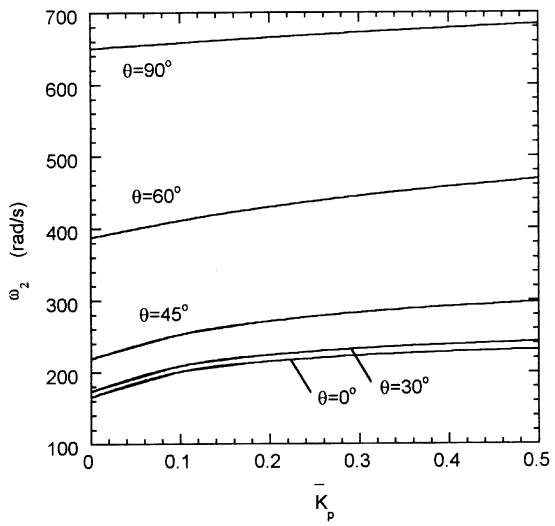

FIGURE 12 The counterpart of Figure 11 for the second coupled eigenfrequency.

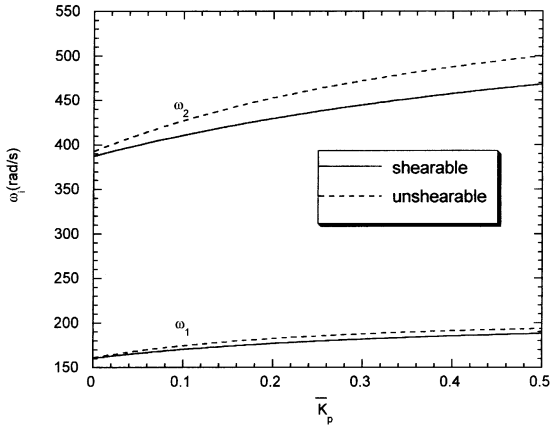

FIGURE 13 Implication of transverse shear on the open ($\overline{K}_p = 0$) and closed-open loop ($\overline{K}_p \neq 0$ first and second eigenfrequencies of the untwisted ($\beta = 0$) rotating blade ($\Omega = 100\,\text{rad/s}$, $\theta = 60°$).

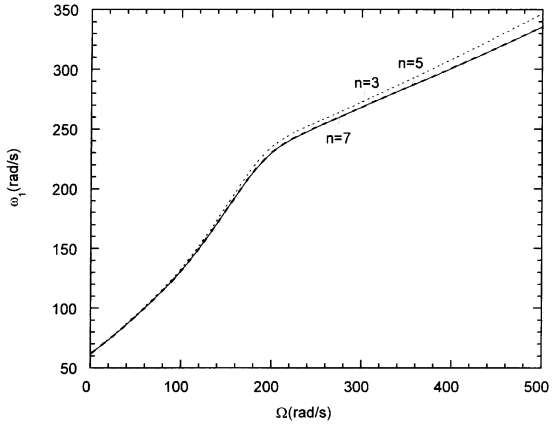

FIGURE 14 Convergence of the solution carried out as per the Extended Galerkin Method for the coupled fundamental eigenfrequency as a function of the rotational speed ($\theta = 45°$, $\overline{K}_p = 0$).

CONCLUDING REMARKS

A dynamical theory of rotating composite blades modeled as thin-walled beams of arbitrary cross-section obtained via the Hamilton's variational principle was supplied.

The theory incorporates a number of non-classical features which are essential for a reliable prediction of free vibration characteristics of advanced rotating composite blades. Among others, the theory includes transverse shear, rotatory inertia, anistropy of constituent materials of the host structure, pretwist, and the adaptive control capability. The strong and synergistic effect played by the directionality property of advanced composite materials considered in conjunction with that of structural pretwist and piezoelectric actuation on their dynamic response characteristics was highlighted.

A powerful and robust solution methodology was used to determine both the open and closed-loop free vibration response characteristics of rotating blades.

It is hoped that in addition to the information provided, the paper can constitute a good basis for further investigation on parametric instability, dynamic response to time-dependent loads, effect of a high temperature field, and aeroelastic flutter instability of blades modeled as thin-walled beams. Such a comprehensive approach of the problem will contribute to the enhancement of the dynamic behavior of these structures, and will ensure the accomplishment of a better design as to avoid the occurence of catastrophic failures of rotor blades (see Srinivasan, 1997).

REFERENCES

Berlincourt, D. A., Curran, D. R. and Jaffe, H. (1964) "Piezoelectric and Piezomagnetic Materials and Their Function in Transducers", *Physical Acoustics – Principles and Methods* (Ed. Mason, E. F.), Vol. 1, Pt. A, Academic Press, New York, pp. 202–204.

Crawley, E. F. (1994) "Intelligent Structures for Aerospace; a Technology Overview and Assessment", *AIAA Journal*, **32**(8), 1689–1699.

Dokumiaci, E., Thomas, J. and Carnegie, W. (1967) "Matrix Displacement Analysis of Coupled Bending–Bending Vibrations of Pretwisted Blading", *Journal Mechanical Engineering Science*, **9**(4), 247–254.

Dosch, J. J., Inman, D. J. and Garcia, E. (1992) "A Self-sensing Piezoelectric Actuator for Collocated Control", *Journal of Intelligent Material Systems and Structures*, **3**(1), 166–184.

Ewins, D. J. and Henry, R. (1992) "Structural Dynamic Characteristics of Individual Blades", *Vibration and Rotor Dynamics*, Von Kármán Institute for Fluid Dynamics, Lecture Series 1992–06, pp. 14.1–14.27.

Kosmatka, J. B. (1992) "Extension-bend-twist Coupling Behavior of Non-homogeneous Anisotropic Beams with Initial Twist", *AIAA Journal*, **30**(2), 519–527.

Librescu, L., Meirovitch, L. and Song, O. (1996) "Integrated Structural Tailoring and Control Using Adaptive Materials for Advanced Aircraft Wings", *Journal of Aircraft*, **33**(1), Jan.–Feb., 203–213.

Librescu, L., Meirovitch, L. and Na, S. S. (1997) "Control of Cantilever Vibration *via* Structural Tailoring and Adaptive Materials", *AIAA Journal*, **35**(8) 1309–1315.

Librescu, L. and Na, S. S. (1998) "Boundary Control of Free and Forced Oscillation of Shearable Thin-walled Beam Cantilevers", *European J. Mech. A/Solids*, **17**(4), 687–700.

Librescu, L., Song, O. and Kwon, H. D. (1999) "Vibration and Stability Control of Gyroelatic Thin-walled Beams *via* Smart Materials Technology", *Smart Structures*, Holnicki-Szulk, J. and Rodellar, J. (Eds.), Kluwer Academic Publication, pp. 163–172.

Librescu, L., Meirovitch, L. and Song, O. (1996) "Refined Structural Modeling for Enhancing Vibrational and Aeroelastic Characteristics of Composite Aircraft Wings", *La Recherche Aerospatiale*, **1**, 23–35.

Rosen, A. (1991) "Structural and Dynamic Behavior of Pretwisted Rods and Beam", *Applied Mechanics Reviews* **44**(12), part 1, 483–515.

Slyper, H. A. (1962) "Coupled Bending Vibrations of Pretwisted Cantilever Beams", *Journal Mechanical Engineering Sciences*, **4**(4), 365–379.

Song, O. and Librescu, L. (1993) "Free Vibration of Anisotropic Composite Thin-walled Beams of Closed Cross-section Contour", *Journal of Sound and Vibration*, **167**(1), 129–147.

Song, O. and Librescu, L. (1997a) "Modeling and Vibration of Pretwisted Spinning Composite Thin-Walled Beams", *Proceedings of the 38th AIAA/ASME/ASCE/AHS/ASC Structures, Structural Dynamics, Materials Conference and Exhibition and AIAA/ASME/AHS/Adaptive Structures Forum*, Paper AIAA 97–1091, Part 1, pp. 312–322, Kissimmee, Florida, April 7–10.

Song, O. and Librescu, L. (1997b) "Structural Modeling and Free Vibration Analysis of Rotating Composite Thin-walled Beams", *Journal of the American Helicopter Society*, **42**(4), 358–369.

Song, O. and Librescu, L. (1999) "Modeling and Dynamic Behavior of Rotating Blades Carrying a Tip Mass and Incorporating Adaptive Capabilities", *Acta Mechanica*, **134**, 169–197.

Song, O. and Librescu, L. (1997c) "Anisotropy and Structural Coupling on Vibration and Instability of Spinning Thin-walled Beams", *Journal of Sound and Vibration*, **204**(3), 477–494.

Srinivasan, A. V. (1997) "Flutter and Resonant Characteristics of Engine Blades", *Journal of Engineering for Gas Turbines and Power, Trans. ASME*, **119**, October, 742–775.

Subrahmanyam, K. B., Kulkarni, S. V. and Rao, J. S. (1981) "Coupled Bending–Bending Vibrations of Pretwisted Blading Allowing for Shear Deformation and Rotary Inertia by the Reissner Method", *International Journal of Mechanical Sciences*, **23**(9), 517–530.

Subrahmanyam, K. B. and Kaza, K. R. V. (1986) "Vibration and Buckling of Rotating Pretwisted, Preconed Beams Including Coriolis Effects", *Journal of Vibration, Acoustics, Stress and Reliability in Design*, **108**, 140–149.

Sunar, M. and Rao, S. S. (1994) "Reent Advances in Sensing and Control of Flexible Structures: *via* Piezoelectric Materials Technology", *Applied Mechanics Reviews*, **52**(1), 1–16.

APPENDIX

The global stiffness quantities including the pretwist effect

$$
\begin{aligned}
a_{22} &= [m^2 a^p_{22} + n^2 a^p_{33} - 2mna^p_{23}],\\
a_{23} &= mn[a^p_{22} - a^p_{33}]\\
a_{25} &= a_{52} = [m^2 a^p_{25} - n^2 a^p_{34} + mn(a^p_{24} - a^p_{35})],\\
a_{33} &= [m^2 a^p_{33} + n^2 a^p_{22} + 2mna^p_{23}]\\
a_{34} &= a_{43} = [m^2 a^p_{34} - n^2 a^p_{25} + mn(a^p_{24} - a^p_{35})],\\
a_{44} &= [m^2 a^p_{44} + n^2 a^p_{55} - 2mna^p_{45}]\\
a_{45} &= mn[a^p_{44} - a^p_{55}],\\
a_{55} &= [m^2 a^p_{55} + n^2 a^p_{44} + 2mna^p_{54}]
\end{aligned}
$$

In addition, the mass terms are given by:

$$b_1 = b^p_1; \quad b_4 = m^2 b^p_4 + n^2 b^p_5 + 2mnb^p_6$$

$$b_5 = m^2 b_5^p + n^2 b_4^p - 2mnb_6^p;$$

$$b_6 = mn[b_5^p - b_4^p];\ b_{13} = mn[b_{14}^p - b_{15}^p],$$

$$b_{14} = m^2 b_{14}^p + n^2 b_{15}^p - 2mnb_{13}^p;$$

$$b_{15} = m^2 b_{15}^p + n^2 b_{14}^p + 2mnb_{13}^p.$$

In these expression, the quantities affected by superscript p are associated with the beam cross-section referred to the principal axes (x^p, y^p), whereas $m(z) \equiv \cos\beta$, $n(z) = \sin\beta$, where $\beta = \beta(z)$. The expressions of stiffness and mass terms referred to principal axes can be found in the paper by Song and Librescu (1997a).